ISSN 1027-4510, Journal of Surface Investigation: X-ray, Synchrotron and Neutron Techniques, 2021, Vol. 15, No. 1, pp. 7–11. © Pleiades Publishing, Ltd., 2021.
Russian Text © The Author(s), 2021, published in Poverkhnost', 2021, No. 1, pp. 10–14.

Study of Nanomaterials for X-Ray Photodynamic Therapy

M. A. Soldatov[a], P. V. Medvedev[a], V. V. Butova[a], V. A. Polyakov[a], I. E. Gorban[a], G. Li[a], and A. V. Soldatov[a, *]

[a] *Smart Materials Research Institute, Southern Federal University, Rostov-on-Don, 344090 Russia*

**e-mail: soldatov@sfedu.ru*

Received February 28, 2019; revised March 22, 2020; accepted March 25, 2020

Abstract—The prototype of an apparatus for studying the X-ray fluorescence properties of nanomaterials for X-ray photodynamic therapy is developed. The X-ray fluorescence characteristics of nanomaterials based on gadolinium fluorides are studied. For a series of samples, X-ray fluorescence spectra are obtained in the region of 600–700 nm, which allows the conclusion that such materials are promising for use as components of radiosensitizers for X-ray photodynamic therapy. The data obtained are important for optimizing the characteristics of nanomaterials and for further modification of the parameters of methods for synthesizing new materials for X-ray photodynamic therapy.

Keywords: nanoparticles, X-ray photodynamic therapy, X-ray fluorescence diagnostics

DOI: 10.1134/S1027451021010146

INTRODUCTION

Oncological diseases in terms of prevalence and fatality rate occupy one of the leading places among socially significant pathologies [1]. Many types of oncological tumors are resistant to certain types of anticancer therapy; therefore, the development of new types of therapy is an extremely important task, especially for the development of approaches to personalized medicine [2]. Photodynamic therapy (in the optical range of radiation) has recently become one of the most important methods for treating a number of oncological tumors close to the surface [2, 3]. However, the rather small effective depth of radiation penetration into tissues significantly limits the list of types of tumors amenable to treatment with photodynamic therapy in the optical range [4]. Unlike radiation in the optical range, higher-energy X-ray and gamma photons easily penetrate the deep tissues of the body [5]. However, at present, there are practically no biocompatible photosensitizers approved for medical use for X-ray and gamma-range photodynamic therapy. X-ray photodynamic therapy is a new field which is promising for use as a treatment of deep tumors [7–17]. The aim of this work is to study the X-ray fluorescence of nanomaterials for their possible use in X-ray photodynamic therapy.

EXPERIMENTAL

To measure X-ray fluorescence, a setup was assembled on the basis of a Phywe X-ray device ($U = 35$ kV, $I = 1$ mA) for X-ray generation and an Agilent Cary Eclipse fluorometer for the detection of X-ray fluorescence spectra. To block off radiation in the visible range from the X-ray spectrum, a 20-μm-thick aluminum foil filter was used. Three different instrument layouts were tested.

In configuration "A" (Fig. 1a), the sample under study in the form of a compressed tablet was placed as close as possible to the X-ray source. The position and orientation of the sample were selected so that the plane of the tablet was at an angle of 45° both to the direction of propagation of X-rays and to the focusing axis of the fluorimeter detector. An X-ray absorbing glass is installed between the test sample and the fluorometer. Due to the proximity of the sample to the X-ray tube, the highest luminosity is achieved. A disadvantage is the protective glass, which absorbs ~15% of the light in the visible region.

In configuration "B" (Fig. 1b), the sample under study was also placed on the X-ray-propagation axis on a specialized holder, printed using a 3D printer. In contrast to configuration "A," the sample under study was located at a greater distance from the X-ray tube. In this configuration, there is no X-ray absorbing glass, which also attenuates the intensity of light transmitted through it in the visible range. However, due to the greater distance from the X-ray tube, the luminescence intensity of the sample is significantly lower than in case "A". To reduce the effect of X-ray radiation on the signal-to-noise ratio, a lead diaphragm was installed in front of the sample.

Configuration "B" (Fig. 1c) is similar to the above configuration. The difference is that the sample is mounted closer to the fluorimeter-detector window and the plane of the tablet is parallel to the plane of the

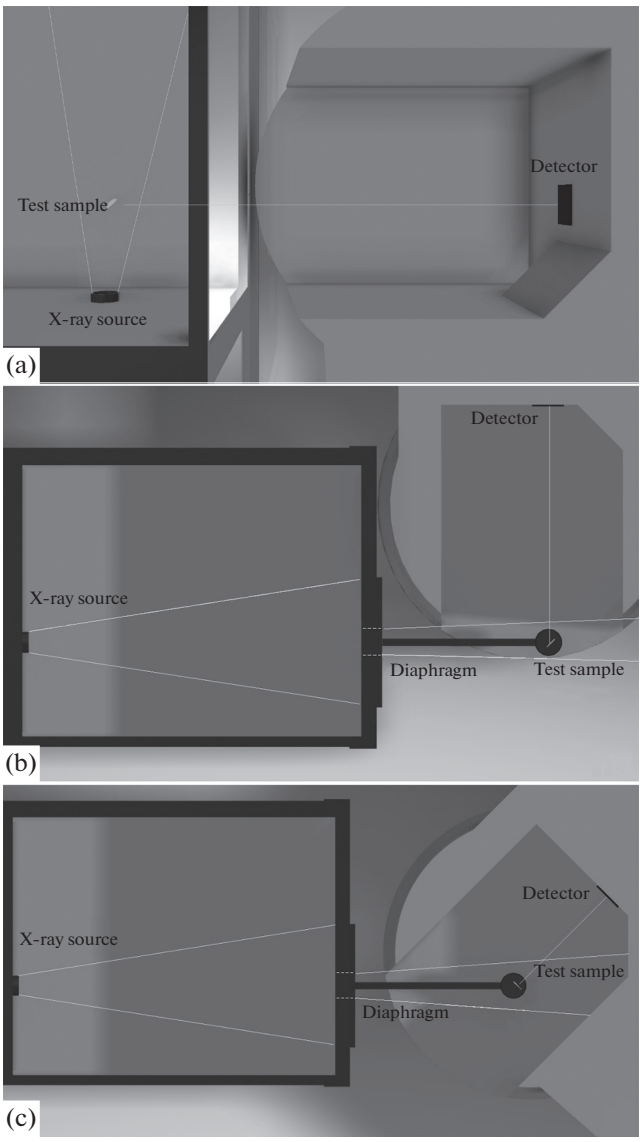

Fig. 1. Installation diagram: a—configuration "A"; b—configuration "B"; c—configuration "C". On the left is the aperture of the X-ray instrument, on the right is a specialized sample holder and the fluorometer cuvette compartment.

detector window. With this measurement method, it was expected that a better signal-to-noise ratio would be obtained due to closer installation of the sample to the intended focus of the fluorimeter. The disadvantage is the increased intensity of X-ray radiation scattered at the walls of the device, which, without protective glass, leads to deterioration in the signal-to-noise ratio.

There are several classes of X-ray phosphors. Nanoparticles doped with ions of the group of rare-earth elements seem to be very promising. Such materials can absorb X-rays and emit quanta in the optical range. A $LiGa_5O_8$:Cr-based nanoscintillator has been proposed, which emits in the near infrared range [18]. This produces optical images of deep tissue that can be used to control exposure. In particular, $LiGa_5O_8$:Cr nanoparticles and a 2,3-naphthalocyanine photosensitizer can be embedded in mesoporous silica nanoparticles. Such nanoconjugates can efficiently accumulate in lung tumors, as evidenced by monitoring of the X-ray luminescence of $LiGa_5O_8$:Cr [18]. It is also of interest to consider a number of compositions doped with Gd^{3+} and Eu^{3+} ions of lanthanide fluorides (e.g. $NaGdF_4$:Eu^{3+}), which make it possible to optimize the radiation parameters under X-ray excitation [19]. It was shown that an attempt to turn on the Ce^{3+} ion in $NaGdF_4$:Eu^{3+} led to a decrease in radiation after X-ray excitation. The surface coating of nanoparticles with a $NaGdF_4$:Eu^{3+} gold shell reduced the X-ray emission in half compared to uncoated phosphors.

$NaGdF_4$:Ce^{3+}, Eu^{3+}—ST synthesis was carried out using the solvothermal method: 0.8 mmol (210.9 mg) of gadolinium(III) chloride, 0.8 mmol (347.3 mg) of cerium(III) nitrate hexahydrate, and 0.8 mmol (206.6 mg) of europium(III) chloride were dissolved in 4 mL of distilled water. 1.6 mmol (412.9 mg) of sodium citrate was separately dissolved in 8 mL of distilled water. The solutions were decanted, and a white precipitate immediately formed. The suspension was heated to a temperature of 90°C and then a solution of 16 mmol (672 mg) of sodium fluoride in 16 mL of distilled water was added. The resulting dispersion was kept for 2 h at a temperature of 90°C. Then the particles were washed three times with distilled water by centrifugation and dried at 60°C. The resulting sample is designated $NaGdF_4$:Ce, Eu. The dried sample was dispersed in 30 mL of distilled water and then placed in a Teflon autoclave. Synthesis was carried out at 210°C for 1 h. The resulting material was washed once again with distilled water and dried at 60°C. The resulting sample is designated $NaGdF_4$:Ce, Eu—ST (solvothermal).

$NaGdF_4$:Ce^{3+}, Eu^{3+}—MV synthesis was carried out by the microwave method: 0.8 mmol (210.9 mg) of gadolinium(III) chloride, 0.8 mmol (197.2 mg) of cerium(III) chloride, and 0.8 mmol (206.6 mg) of europium(III) chloride were dissolved in 4 mL of distilled water. 1.6 mmol (412.9 mg) of sodium citrate was separately dissolved in 8 mL of distilled water. The solutions were decanted, and a white precipitate immediately formed. The suspension was heated to 90°C and then a solution of 16 mmol (672 mg) of sodium fluoride in 16 mL of distilled water was added. The resulting dispersion was kept for 2 h at a temperature of 90°C. The mixture was then transferred to a Teflon cell and placed in a CEM Mars6 microwave oven. The microwave synthesis conditions were: temperature rise time of 20 min, holding time of 1 h, temperature of 210°C, and a power of 600 W. The resulting material was washed three times with distilled water

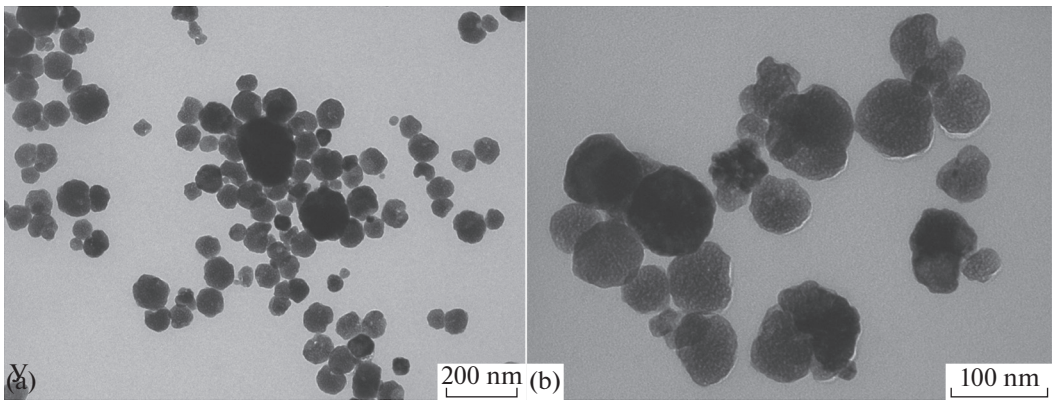

Fig. 2. $NaGdF_4$: Ce, Eu–MV images, obtained in a transmission electron microscope at different magnifications.

and dried at 60°C. The sample was designated $NaGdF_4$: Ce, Eu–MB (microwave).

RESULTS AND DISCUSSION

The average size of the synthesized nanoparticles does not exceed 100 nm (Fig. 2). As seen from the X-ray diffraction patterns, the synthesized $NaGdF_4$ samples are a mixture of phases, the main one is the hexagonal phase α-$NaGdF_4$ (Fig. 3). The broadening of the peaks is associated with the fine particle size. The precipitate obtained at a temperature of 90°C corresponds to a single-phase product; however, upon additional processing in an autoclave, a phase transition is observed. In the sample $NaGdF_4$:Ce, Eu–MV, two phases are identified: hexagonal α-$NaGdF_4$ (from PDF database #27-0699) and cubic β-$Gd_4F_6O_3$ (#27-0697).

When measuring the X-ray fluorescence, a more intense signal for a standard X-ray phosphor was obtained in the case of configuration "A". Therefore, all measurements were performed using this configuration. The distance of the sample from the X-ray photon source and optical radiation detector, as well as the low power of the source ($U = 35$ kV, $I = 1$ mA) were a significant limitation in the measurements. Nevertheless, X-ray fluorescence spectra were successfully recorded for a number of samples based on gadolinium fluorides (Fig. 4).

When analyzing the X-ray fluorescence spectra, the background spectrum (with a maximum at 660 nm) measured with the X-ray source turned off was subtracted. The X-ray fluorescence spectra were analyzed by averaging the signal over the points and then fitting the peaks using the Gaussian function. It was found that the X-ray fluorescence spectrum of the

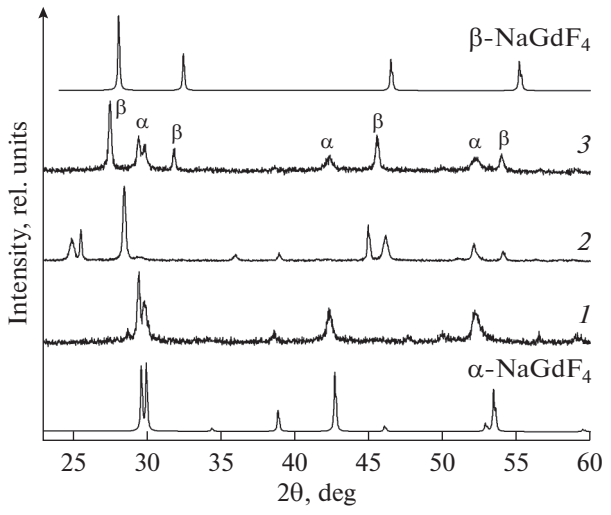

Fig. 3. Diffraction patterns of the synthesized samples: $NaGdF_4$:Ce, Eu (*1*), $NaGdF_4$:Ce, EuST (*2*), $NaGdF_4$:Ce, Eu–MV (*3*).

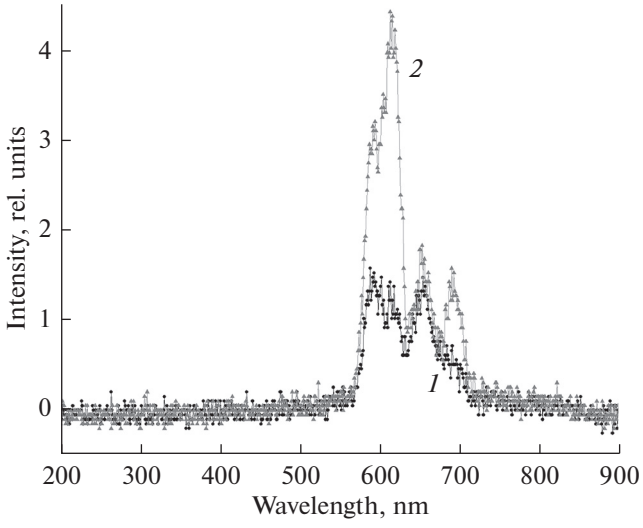

Fig. 4. X-ray fluorescence spectra of the samples based on gadolinium fluorides: *1*—$NaGdF_4$:Eu^{3+}–ST, *2*—$NaGdF_4$:Eu^{3+}–MV.

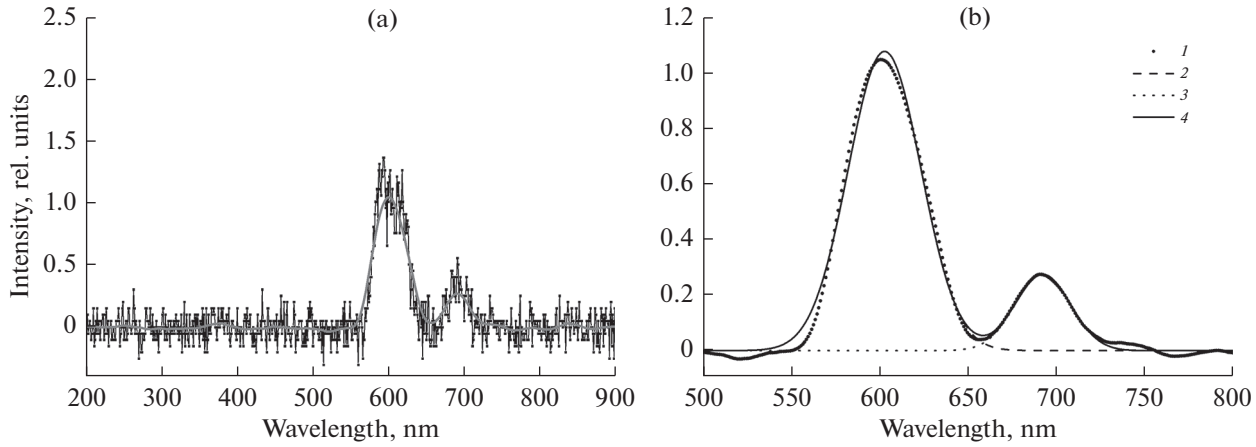

Fig. 5. X-ray fluorescence spectrum of $NaGdF_4:Eu^{3+}$–ST material (a): points – experiment; solid line – experimental data averaging. Fitting results using the Gaussian function (b): *1*—averaging of experimental data; *2*—contribution of the peak at 603 nm; *3*—contribution of the peak at 693 nm; *4*—fitting results.

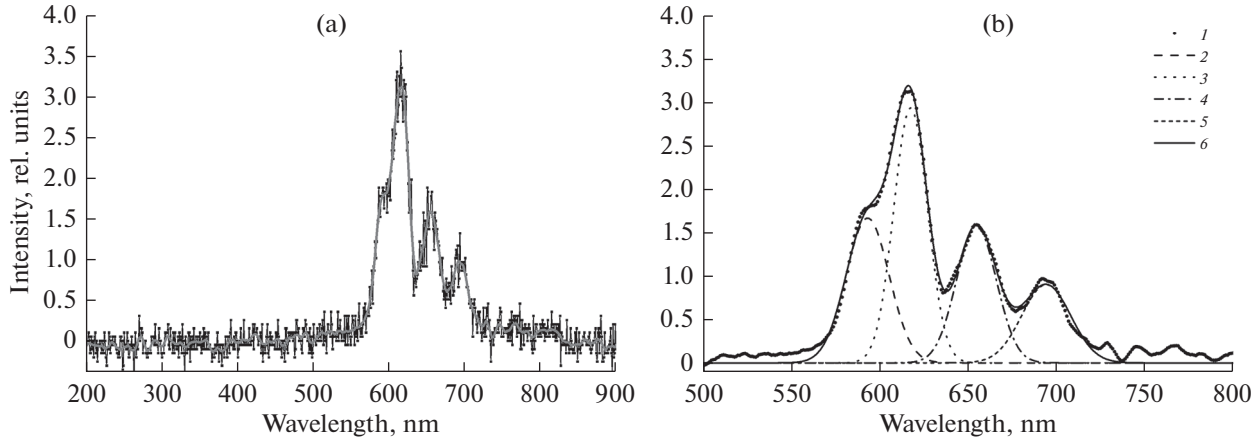

Fig. 6. X-ray fluorescence spectrum of $NaGdF_4:Eu^{3+}$–MV material (a): points – experiment; solid line – averaging of experimental data. Fitting results using the Gaussian function (b): *1*—averaging of experimental data; *2*—contribution of the peak at 593 nm; *3*—contribution of the peak at 618 nm; *4*—contribution of the peak at 655 nm; *5*—contribution of the peak at 694 nm; *6*—fitting results.

$NaGdF_4:Eu^{3+}$–ST sample has maxima at wavelengths of 603 and 693 nm (Fig. 5).

The highest X-ray fluorescence yield was obtained for the $NaGdF_4:Eu^{3+}$–MV sample. After fitting the four peaks with a Gaussian function, it was found that the fluorescence maxima are at the wavelengths 593, 618, 655, and 694 nm (Fig. 6). It should be noted that the main contribution to the spectrum is made by transitions $^5D_0 \rightarrow {}^7F_J$ with Eu^{3+} emission at wavelengths of 587, 612, ~700 nm [6]. Apparently, due to the low intensity of the X-ray source, the peaks at 587 and 612 nm could not be separated for the $NaGdF_4:Eu^{3+}$–ST sample. The contributions of the peaks at 593, 618, 655, and 694 nm for the $NaGdF_4:Eu^{3+}$–MV sample were separated.

CONCLUSIONS

For a series of samples based on gadolinium fluorides, X-ray fluorescence spectra were obtained in the range of 600–700 nm, which suggests that such materials are promising for use as a component of radiosensitizers for X-ray photodynamic therapy. The data obtained are important for optimizing the characteristics of nanomaterials and for further modifying the parameters of methods for synthesizing new materials for X-ray photodynamic therapy.

FUNDING

The study was carried out with support of the Russian Science Foundation (project No. 19-15-00305).

REFERENCES

1. W. K. Kelly and S. Halabi, *Oncology Clinical Trials* (Springer, Berlin, 2018).
2. W. Fan, P. Huang, and X. Chen, Chem. Soc. Rev. **45,** 6488 (2016). https://doi.org/10.1039/c6cs00616g
3. G. Yi, S. H. Hong, J. Son, et al., Quant. Imaging Med. Surg. **8,** 433 (2018).
4. A. Kamkaew, F. Chen, Y. Zhan, et al., ACS Nano **10** (4), 3918. https://doi.org/10.1021/acsnano.6b01401
5. X. Zhang, S. Zhu, Y. Li, et al., Biomed. Eng. Online **17,** 45 (2018). https://doi.org/10.1186/s12938-018-0480-x
6. L. Sudheendra, K. D. Gautom, Ch. Li, et al., Chem. Mater. **26,** 1881 (2014). https://doi.org/10.1021/cm404044n
7. M. Sivasubramanian, Y. C. Chuang, and L. W. Lo, Molecules **24,** 520 (2019). https://doi.org/10.3390/molecules24030520
8. L. Larue, A. Ben Mihoub, Z. Youssef, et al., Photochem. Photobiol. Sci. **17,** 1612 (2018). https://doi.org/10.1039/c8pp00112j
9. B. W. Pogue and B. C. Wilson, J. Biomed. Opt. **23,** 1 (2018). https://doi.org/10.1117/1.JBO.23.12.121610
10. M. Misawa and J. Takahashi, Nanomedicine **7,** 604 (2011). https://doi.org/10.1016/j.nano.2011.01.014
11. A. H. Elmenoufy, Y. Tang, J. Hu, et al., Chem. Commun. **51,** 12247 (2015). https://doi.org/10.1039/c5cc04135j
12. W. Fan, P. Huang, and X. Chen, Chem. Soc. Rev. **45,** 6488 (2016). https://doi.org/10.1039/c6cs00616g
13. H. Chen, G. D. Wang, Y. J. Chuang, et al., Nano Lett. **15,** 2249 (2015). https://doi.org/10.1021/nl504044p
14. W. Fan, W. Tang, J. Lau, et al., Adv. Mater. **31,** 1806381 (2019). https://doi.org/10.1002/adma.201806381
15. B. Cline, I. Delahunty, and J. Xie, WIREs Nanomed. Nanobiotechnol. **11,** 1541 (2019). https://doi.org/10.1002/wnan.1541
16. S. Kaščáková, A. Giuliani, S. Lacerda, et al., Nano Res. **8,** 2373 (2015). https://doi.org/10.1007/s12274-015-0747-5
17. H. P. Chen, F. I. Tung, M. H. Chen, and T. Y. Liu, J. Controlled Release **226,** 182 (2016). https://doi.org/10.1016/j.jconrel.2016.02.025
18. H. Chen, X. Sun, G. D. Wang, et al., Mater. Horiz. **4,** 1092 (2017). https://doi.org/10.1039/C7MH00442G
19. L. Sudheendra, G.K. Das, C. Li, et al., Proc. SPIE **8596,** 85960D (2013). https://doi.org/10.1117/12.2005250

SPELL: 1. OK